The quest for function in systems with two dynamic covalent bonds

Marić, Ivana

DOI:
10.33612/diss.167788912

4.

New Hydrazide Peptide Building Blocks: to Fold or Not to Fold, Therefore Self-Replicate?

This chapter contains parts of *submitted* article:
C. G. Pappas, B. Liu, I. Marić, J. Ottelé, A. Kiani, M. L. van der Klok, P. R. Onck, S. Otto. Two Sides of the Same Coin: Emergence of Foldamers and Self-Replicators from Dynamic Combinatorial Libraries.

4.1 Introduction

In life, as we know it, three basic types of biopolymers (polypeptides, polynucleotides, and polysaccharides) are ascribed as fundamental players. These molecules mediate functions that underlie extant life but also are able to self-preserve stability by acquiring specific conformations. Such states are regarded as *folded*, where a particular structure is formed by the cooperative action of various intrachain non-covalent interactions or *assembled*, in which association occurs between the same or different biopolymer types.[1] The universal approach to conformational and functional persistence among classes of biopolymers points in the direction of their simultaneous emergence and co-evolution.[2,3]

Proteins, the mediators of catalytic processes, and nucleic acids, molecules that store and copy genetic information, are prime examples of folded and assembled structures, respectively. Although very strictly divided in terms of labor and structure, both types of molecules are found at the functional interplay of the central dogma of biology, being part of the machinery associated with the translation of genetic information into catalytically active systems.[4] Additionally, chemical alterations of proteins that emerge from biosynthetic pathways can occur to add variation and diversity to the functional groups beyond those present in the side chains of the 20-22 proteinogenic amino acids. These chemical alterations are regarded as post-translational modifications (PTMs). They can help mediate folding into a proper conformation, increase the stability or promote localization of the protein to a distinct cellular compartment, alter or turn "on" and "off" biological activity of an enzyme, etc. Overall, PTMs expand nature's repertoire by increasing the toolbox while maintaining the amount of genetic information limited.[5]

Due to their importance in biochemistry, self-replication[6] and foldamer formation[7] have been increasingly investigated also in purely synthetic settings in the past few decades. Since von Kiedrowski's seminal work on minimal self-replicating systems,[8] examples, including RNA[9] and peptides[10] have been designed and studied. We have extensively researched a systems chemistry approach towards the emergence of self-replicating molecules from complex mixtures of interconverting molecules.[11] The field of artificial folded molecular structures proved beneficial in understanding how proteins fold into native conformations and the relationships between the structures and functional behavior.[12] Even more challenging and interesting, chemists have shown that it is possible to design folded polymers with functional and organizational properties not precedented in nature.[13] Both natural and non-biological precursors have been exploited to produce

foldamers via stepwise synthesis.[14] In contrast, our group has reported the successful use of a dynamic combinatorial method enabling the spontaneous emergence of discrete architectures of remarkable structural complexity.[15,16] In this approach, intramolecular interactions among recurrent elements drive the folded structure formation. Thus far, the processes of self-replication and folding have been independently studied. However, in nature, these two processes share strong connectivity, and recently, but also in this chapter we show that a relationship in synthetic systems could be established as well.[17,18]

In this chapter, we attempt to build on pioneering work[16] by Pappas *et al.*, who revealed that dipeptide-dithiol appended molecules could spontaneously self-assemble into complex discrete folded structures. For those building blocks that yielded foldamers, it has been shown that 3,5-dimercaptobenzene-derived oligomeric macrocycle collaps to form a dense hydrophobic core as observed in globular proteins, while the dipeptides occupy peripheral positions and form multiple hydrogen bonds. The authors also observed that molecules with a particular fold could be amplified at the expense of other library members upon introducing a template. Having a constitutionally dynamic foldamer with a hydrophobic core and affinity for binding another molecule in hand, we hypothesized that these molecules could be suitable platforms for developing synthetic functional foldamers that serve as catalysts. The research presented here also aimed to make use of the post-modification strategy developed and elaborated in **Chapter 3**, which would allow placing different catalytically active functionalities in a hydrophobic environment without elaborate synthesis. Thus, the three building blocks reported previously **1**, **2,** and **3** (**Scheme 4.1a**), that gave rise to $\mathbf{1}_{23}$ and large families of oligomers were hydrazide-functionalized at the C-terminus and the behaviour of corresponding molecules **4**, **5** and **6** (**Scheme 4.1b**) in dynamic combinatorial libraries was investigated. We found that even minute changes in the chemical structure of building block (such as hydrazide functionalization of C-terminus) can change the system's outcome from folding towards replication as molecules **4**, **5** and **6** yielded fibrous-like self-replicating assemblies. We also investigated whether the system that initially self-replicates can be directed towards folding by employing different strategies. Foldamer formation of hydrazide-functionalized molecule **4** was achieved, only in the presence of a large mole fraction of the carboxylate building block **1** (i.e., 90% of **1**), to yield mixed 23mer species. We also show that dynamic reconfiguration of foldamer to self-replicator is possible by a series of partial reduction/oxidation steps of the library that was initially dominated by a folded structure. This result suggests that the processes of folding and self-replication are related in these synthetic systems and underlines the difficulties in designing molecules for a predetermined, specific outcome.

4.2 Results and Discussion

4.2.1 The Rationale Behind the Selection of Dipeptide-Dithiol Building Blocks for Hydrazide-Functionalization

Encouraged by the recent discovery of new foldamers via a dynamic combinatorial approach, we aimed to implement novel functions or induce reconfiguration due to new non-covalent interactions by post-assembly modification. From the already explored structural space, we have chosen molecules **1-3** that appeared as interesting candidates for further modification and study. All three building blocks feature amphiphilic amino-acid side chains. Structure **1** bears a dipeptide chain, composed of modified phenylalanine (*p*-NH_2 substituted) and a lysine amino-acid residue. Upon oxidation and disulfide exchange, **1** spontaneously organizes into a folded macrocycle consisting of 23 identical units, $\mathbf{1}_{23}$. The structural resemblance between the amino-substituted segment of **1** and aniline, a known organocatalyst for hydrazone formation,[19] prompted us to functionalize this building block with the hydrazide group, envisioning that the resulting molecule (i.e., **4**) would assemble into a foldamer that can catalyse the production of the very molecules it needs to fold (i.e., its own "food" based on acyl-hydrazone adduct of **4** and an **aldehyde**). Zwitterionic molecules **2** and **3** (at working pH) gave rise to a family of large non-selective rings (from 9 to 22 components in a single macrocycle). Thus, we hypothesized that by charge-tuning, as in cationic molecules **5** and **6**, a transition to selective macrocycle formation can be achieved. Subsequently, the foldamers of **5** and **6** could undergo post-modification at the NH-NH_2-functionalized C-terminus by a small aldehyde to potentially yield a catalytically active foldamer.

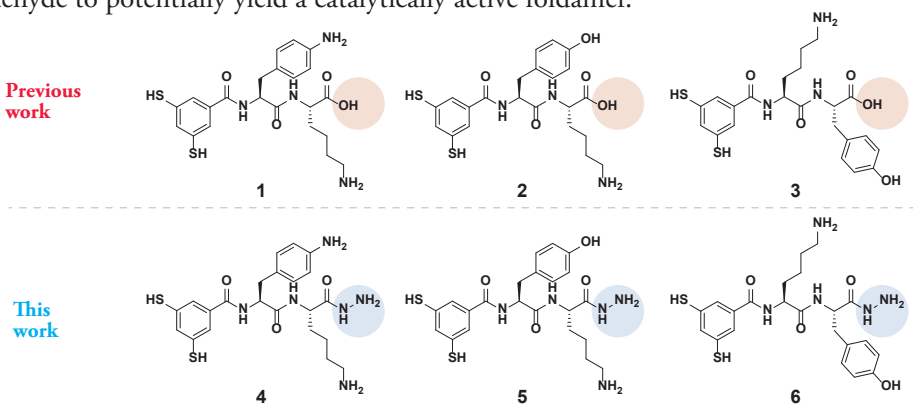

Scheme 4.1 Chemical structures of previously reported carboxylate-functionalized peptide building blocks **1**, **2** and **3**, that give rise to the foldamer $\mathbf{1}_{23}$ and families of large oligomers, respectively, and hydrazide-functionalized peptide building blocks **4**, **5** and **6** investigated in the current study.

4.2.2 The Emergence of Self-Replicators with Fiber-Like Structures

To investigate the emergent behavior of chemical systems based on molecules **4**, **5** and **6**, the three dynamic combinatorial libraries from each building block (4 mM in 50 mM borate buffer, pH 8.2) were prepared. We monitored the distribution of species in the DCLs by Ultra Performance Liquid Chromatography/Mass Spectrometry (UPLC/MS) analysis for 3 to 13 days, depending on the building block. In the initial phases, all three DCLs were composed of linear dimers and macrocycles containing 3 and 4 monomeric units following the fast perborate-mediated oxidation. Upon allowing libraries to equilibrate, through air-mediated oxidation and disulfide exchange processes, growth in the concentration of $\mathbf{4}_6$, $\mathbf{5}_5$ and $\mathbf{6}_6$ took place. Kinetic data in **Figure 4.1a** shows the emergence of $\mathbf{4}_6$ shortly after the library was prepared. At the same time, the sigmoidal shape of the growth curve for $\mathbf{5}_5$ (**Figure 4.1c**) and $\mathbf{6}_6$ (**Figure 4.1e**) is indicative of replication behavior. Additionally, the size of macrocycles generated as dominant species in these DCLs points in the direction of the formed molecules being self-replicators rather than foldamers. To verify whether the molecules $\mathbf{4}_6$, $\mathbf{5}_5$ and $\mathbf{6}_6$ can catalyze their own formation, we performed a typical seeding experiment. Thus, 15 mol% of the preformed seeds of $\mathbf{4}_6$, $\mathbf{5}_5$ and $\mathbf{6}_6$ were added to partially oxidized libraries made from the corresponding monomers. The UPLC analysis showed that the time scale of the emergence of the suspected self-replicating species was shortened when compared to the non-seeded libraries, confirming the autocatalytic nature of the formation of $\mathbf{4}_6$, $\mathbf{5}_5$ and $\mathbf{6}_6$ (**Figure 4.1b**, **d** and **f**). Such behavior is, in particular, evident for the growth curves of $\mathbf{5}_5$ and $\mathbf{6}_6$, as seeding bypasses the lag phase. The time difference in the emergence of $\mathbf{6}_6$ between experiments where the kinetic profile was followed (**Figure 4.1e**, approximately 60% with respect to monomer **6**) and seeding experiments (**Figure 4.1f**, approximately 75% with respect to monomer **6**) most likely originates from variability in levels of oxidation of libraries.

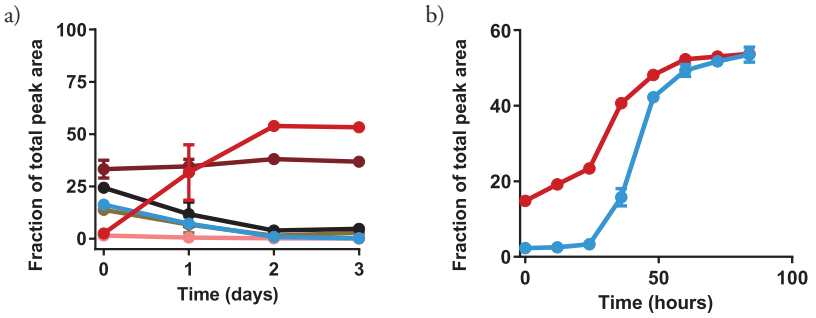

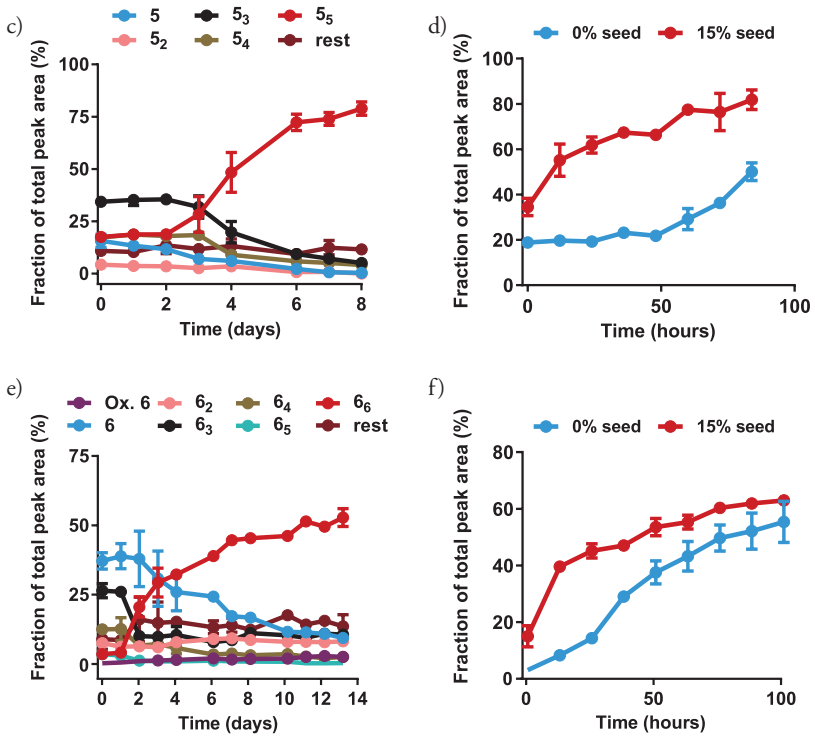

Figure 4.1 a), **c)** and **e)** Kinetic profiles (monitored at 254 nm) of formation of self-replicators $\mathbf{4}_6$, $\mathbf{5}_5$ and $\mathbf{6}_6$ starting from building blocks **4**, **5** and **6**, respectively (4.0 mM) in borate buffer (50 mM, pH 8.2), stirred at 1200 rpm. Libraries based on **4** and **5** were oxidized to 80%, and on **6** to 60%, with respect to monomer (with 40 mM sodium perborate solution) and left to equilibrate under ambient atmosphere. **b)**, **d)** and **f)** Comparison of the growth of self-replicators in non-seeded and seeded libraries with 15 mol% of seed (monitored at 254 nm): **b)** $\mathbf{4}_6$, **d)** $\mathbf{5}_5$ and **f)** $\mathbf{6}_6$. Libraries were prepared at 4.0 mM concentration in the corresponding building blocks, in borate buffer (50 mM, pH 8.2) and stirred at 1200 rpm. Both non-seeded and seeded libraries were oxidized between 75% and 85% with respect to monomer. The temperature was kept constant at 25°C throughout all experiments. The graphs are based on 3 independent replicates.

TEM and AFM analysis show that in all three DCLs, when dominated by self-replicators $\mathbf{4}_6$, $\mathbf{5}_5$ and $\mathbf{6}_6$, fibrous, supramolecular polymers were present (**Figure 4.2a-f**). Both types of micrographs depict associated fibers, particularly for the assemblies $\mathbf{5}_5$ and $\mathbf{6}_6$, where strong lateral association led to the formation of aggregates (**Figure 4.2c** and **Figure 4.2f**). As the libraries based on building blocks **5** and **6** were progressing towards the self-assembled organization, the turbidity of samples increased, which correlates with aggregate formation. This is possibly due to the relatively high salt concentration present in the solution, as the DCLs were prepared in 50 mM borate buffer (50 mM in $B_4O_7^{2-}$).

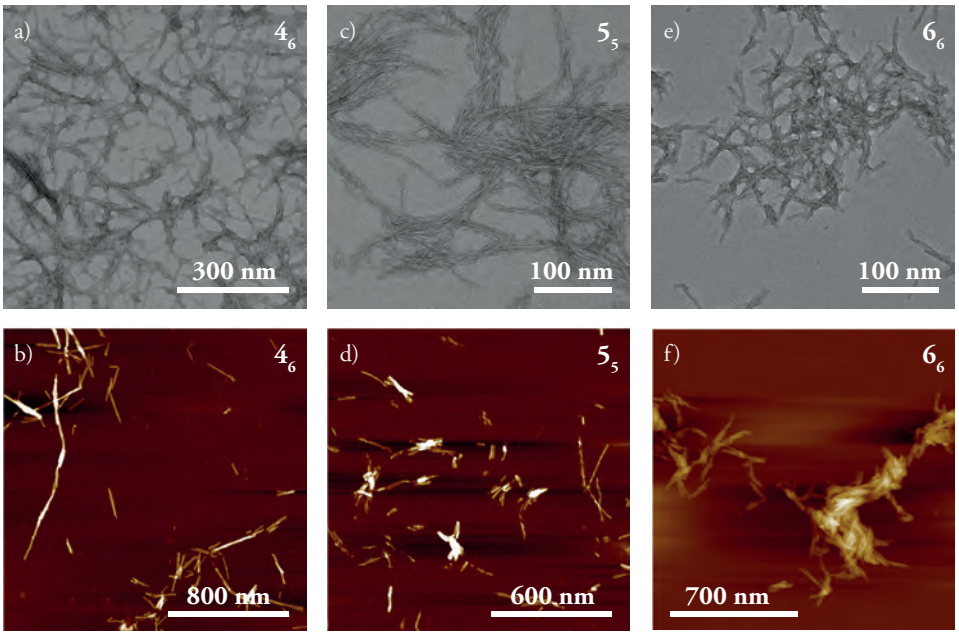

Figure 4.2 Negative stain transmission electron micrographs (top row) and atomic force micrographs (bottom row) of DCLs obtained by oxidation of **a)** and **b) 4** when dominated by $\mathbf{4}_6$; **c)** and **d) 5** when dominated by $\mathbf{5}_5$ and **e)** and **f) 6** when dominated by $\mathbf{6}_6$.

In summary, we speculate that increasing charge repulsion between the building blocks by providing them with a permanent net charge (resulting from the protonated lysine amino-acid residue, while the C-terminus is not charged as pK_a values of hydrazides are 4-5[20]) favoured replicator over foldamer formation. Such an outcome suggests a design rule for foldamers in terms of electrostatics; molecules that do not exhibit net charge, thus do not suffer from charge repulsion between the repeating units, are more likely to give rise to compact foldamer structures.

4.2.3 Characterization of Fibrous Self-Replicators

Circular dichroism (CD) was employed to characterize the fibrous self-replicators further, as this technique provides information about the structural organization of assemblies. The solutions of the self-replicators show two intense negative bands at 270 nm and 220 nm and a positive band at 200 nm (**Figure 4.3a, c** and **e**), which are indicative of β-sheet assembly.[21] Additionally, the appearance of bands with higher intensities for $\mathbf{4}_6$, $\mathbf{5}_5$ and $\mathbf{6}_6$ when compared with their monomers suggests the formation of well-defined assemblies,

where the aromatic cores of the hexamer or pentamer macrocycles are stacked in a chiral manner.

Thioflavin T (ThT) fluorescence assay was used to confirm that species $\mathbf{4}_6$, $\mathbf{5}_5$ and $\mathbf{6}_6$ acquire ordered β-sheet structures. The ThT fluorescence signal at 490 nm showed the increase in the presence of DCLs dominated by self-replicators $\mathbf{4}_6$, $\mathbf{5}_5$ and $\mathbf{6}_6$ (150-fold for **4**, 500-fold for **5** and 100-fold for **6**) compared to blank samples (**Figure 4.3b**, **d** and **f**), confirming the formation of well-organized structures capable of binding the ThT molecules.

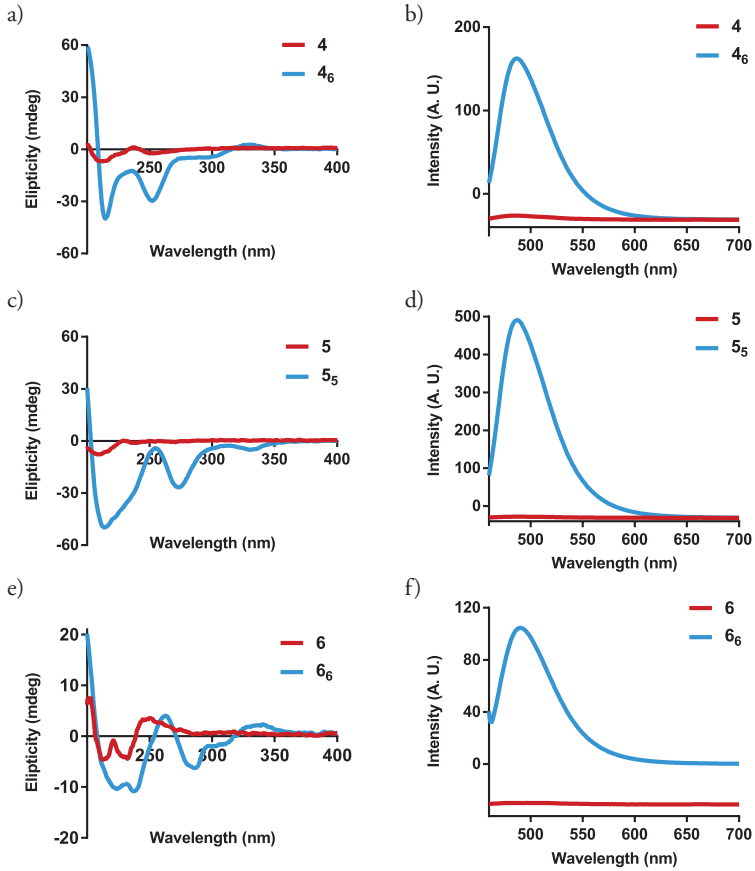

Figure 4.3 CD spectra (blue lines) of DCLs obtained by oxidation of **a) 4** when dominated by $\mathbf{4}_6$; **c) 5** when dominated by $\mathbf{5}_5$ and **e) 6** when dominated by $\mathbf{6}_6$. The enhancement of CD signals for self-assemblies $\mathbf{4}_6$, $\mathbf{5}_5$ and $\mathbf{6}_6$ is evident compared to the CD spectra of the corresponding building blocks in the monomer state, given as red lines. Thioflavin T fluorescence emission spectra (blue lines) of DCLs obtained by oxidation of **b) 4** when dominated by $\mathbf{4}_6$; **d) 5** when dominated by $\mathbf{5}_5$ and **f) 6** when dominated by $\mathbf{6}_6$. The enhancement of ThT signals for self-assemblies $\mathbf{4}_6$, $\mathbf{5}_5$ and $\mathbf{6}_6$ is evident compared to the ThT spectra of the corresponding building blocks in the monomer state, given as red lines.

4.2.4 Exploring Strategies to Depart from Self-Replication Towards Folding

As hydrazide-functionalized peptide building blocks **4**-**6** do not yield foldamers but rather self-replicate, a couple of strategies that might lead to the foldamer formation have been explored.

4.2.4.1 The Influence of Mechanical Forces on the Product Distribution in DCLs

The elongation-breakage step, promoted by mechanical energy, is essential for the self-replication process in systems based on dithiol-peptide molecules.[22] We hypothesized that in the absence of stirring, the system would not undergo the secondary nucleation step, circumventing the self-replication, which in return would allow molecules to find a suitable conformation in a folded assembly. To test whether foldamers can be obtained in this manner, three libraries of molecules **4**, **5** and **6** (4.0 mM) were prepared in borate buffer (50 mM, pH 8.2) and not agitated. As a control, three libraries of identical starting composition were prepared and stirred at 1200 rpm. After 10 days (for building block **4**) and 8 days (for building blocks **5** and **6**), UPLC/MS analysis of control DCLs showed the presence of corresponding self-replicators as major products, while in non-stirred samples, trimers, tetramers and other non-assembling species were the dominant compounds (**Figure 4.4**). Self-replicators $\mathbf{4}_6$, $\mathbf{5}_5$ and $\mathbf{6}_6$ were also identified in non-stirred DCLs, yet in lower amounts, indicating that absence of agitation does not completely prevent replicator formation but rather slows it down. Besides, no larger macrocycles that could acquire folded conformation were detected in any of the three non-stirred libraries. This suggests that building blocks **4**, **5** and **6** cannot be directed towards foldamers, i.e., away from self-replicating structures, by altering mechanical energy input.

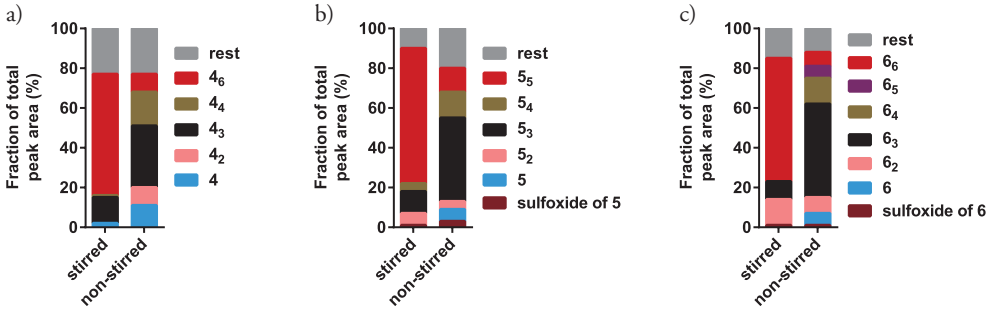

Figure 4.4 Effect of stirring (stirred at 1200 rpm and without agitation) on product composition of DCLs made from building blocks: **a) 4** (4.0 mM) in borate buffer (50 mM, pH 8.2) on day 10; **b) 5** (4.0 mM) in borate buffer (50 mM, pH 8.2) on day 8 and **c) 6** (4.0 mM) in borate buffer (50 mM, pH 8.2) on day 8.

4.2.4.2 The Influence of Salts on the Product Distribution in DCLs

By using the intrinsic advantage of dynamic combinatorial chemistry i.e., the fact that library members that engage in non-covalent interactions are favoured over their less strongly interacting counterparts, we investigated whether molecular-recognition-induced changes in library composition can be large enough to allow identification of new foldamers. Additionally, the presence of salt should enhance the hydrophobic effect, i.e., favour the structure in which the hydrophobic surfaces are buried, and the hydrophilic side chains are exposed to the solvent.[23] Thus, libraries of **4**, **5** and **6** (2.0 mM) were prepared in borate buffer (50 mM, pH 8.2) and in the presence of the following salts NaF, $NaCH_3COO$, NaCl and NaSCN (1.0 M) as templates. The identified species are analogous to the already reported products of DCLs based on **4** and **6**, with the corresponding self-replicators being the major products (**Figure S4.30a** and **S4.31**). The only exception was the formation of $\mathbf{5}_{16}$, in the library prepared from **5** in the presence of NaCl (**Figure S4.30b**). However, the addition of sodium salts led to the significant loss of peak area regardless of the combination of building block and template, posing a challenge for reliable analysis of these libraries, as evident from the UPLC measurements. In conclusion, the change in environmental conditions, i.e., ionic strength, affected the qualitative outcome only of the library made from **5**, although accompanied by precipitation.

4.2.4.3 Systems of Mixed Building Blocks as Potential Platforms or Foldamer Formation

Since altering experimental conditions showed to be an unsuccessful strategy for foldamer formation and having two structurally similar molecules in hand that give either foldamers (for **1**) or replicators (for **4**), we set out to investigate the DCL behaviour made by mixing these two building blocks. A library containing 90 mol% of **1** and 10 mol% of **4** (at a total concentration of 2.0 mM in 50 mM borate buffer, pH 8.2) was prepared and stirred in air. After 14 days, we observed mixed 23mers, eventually accounting for up to 75% of the library material (**Figure 4.5a-b**). Separation of the large mixed macrocycles proved to be challenging with the available chromatographic techniques. However, MS analysis (**Figure S4.33**) confirms that the family of large macrocycles is composed of a series of mixed 23mers, even though we cannot identify their exact composition. The CD spectrum of the DCL formed by mixing the two building blocks is identical to the one recorded for $\mathbf{1}_{23,}$ confirming the presence of mixed 23mers as indicated by mass spectrometry (**Figure 4.5c**).

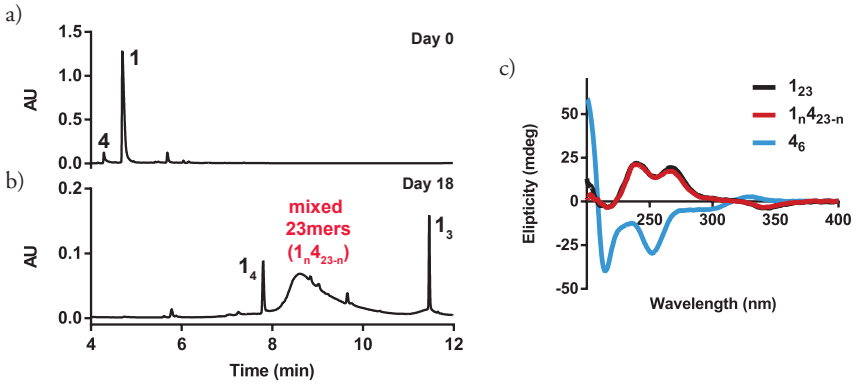

Figure 4.5 UPLC analyses of a DCL made by oxidation of **1** and **4** (at a total concentration of 4.0 mM, 90:10 ratio) in borate buffer (12.5 mM, pH 8.2) **a)** immediately after dissolving and **b)** after stirring for 19 days. **c)** CD spectra of DCLs dominated by $\mathbf{1}_{23}$ (black line), **mixed 23mers** (red line) and $\mathbf{4}_{6}$ (blue line).

Thus, the strategy to shift away from self-replication towards the foldamers containing building block **4** by incorporating more of the molecule that tends to fold, i.e., **1**, showed to be successful. Here, the folding propensity of **1** dominated the system and guided it towards the targeted outcome. The potential of the mixed foldamers with the possibility to be post-modified remains to be explored, with some possible applications being catalysis and reconfiguration of assembly.

4.2.5 Dynamic Transition from Folding to Self-Replication

Previously, it was found that molecule $\mathbf{1}_{6}$ can emerge and self-replicate only upon chemical changes in environmental conditions, such as salt addition.[17] Puzzled by the ability of the system to fold, as well as replicate (**1**: $\mathbf{1}_{23}$ and $\mathbf{1}_{6}$), while the other system only formed a replicator (**4**: only $\mathbf{4}_{6}$), we hypothesized that the foldamer $\mathbf{1}_{23}$ might be a kinetically trapped product, while self-replicator $\mathbf{1}_{6}$ is the thermodynamic minimum of the energy landscape. Thus, we set out to uncover whether *in situ* dynamic reconfiguration of foldamer to self-replicator is possible. A library of **1** at a total concentration of 2.0 mM in borate buffer (12.5 mM, pH 8.0) was set up and monitored using UPLC/MS. Species $\mathbf{1}_{23}$ was the dominant product, while low amounts of $\mathbf{1}_{3}$ and $\mathbf{1}_{6}$ were also detected (**Figure 4.6a**). Based on this outcome, it appears that the rate of foldamer formation is higher than that of the nucleation step of the self-replication process, resulting in the foldamer out-competing the self-replicator. However, when the library dominated by $\mathbf{1}_{23}$ was subjected to a series of partial reduction/oxidation steps (**Figure S4.34**), an increase in the amount of $\mathbf{1}_{6}$ was observed with each reduction step (**Figure 4.6b-d**). After four

sequential partial reductions, a complete conversion of foldamer $\mathbf{1}_{23}$ to self-replicator $\mathbf{1}_6$ was achieved (**Figure 4.6e**), suggesting that the self-replicating structure most likely represents the system's lowest energy state (**Figure 4.6f**). Interestingly, by comparing peak areas of $\mathbf{1}_6$ and $\mathbf{1}_{23}$ before and after reduction (**Figure S4.35**), we also observed that replicator $\mathbf{1}_6$ is more resistant to reduction than $\mathbf{1}_{23}$. This indicates that disulfide bridges of foldamer, although buried within the hydrophobic core, are more readily accessible than bonds that keep the rings within the monomeric supramolecular fibers together.

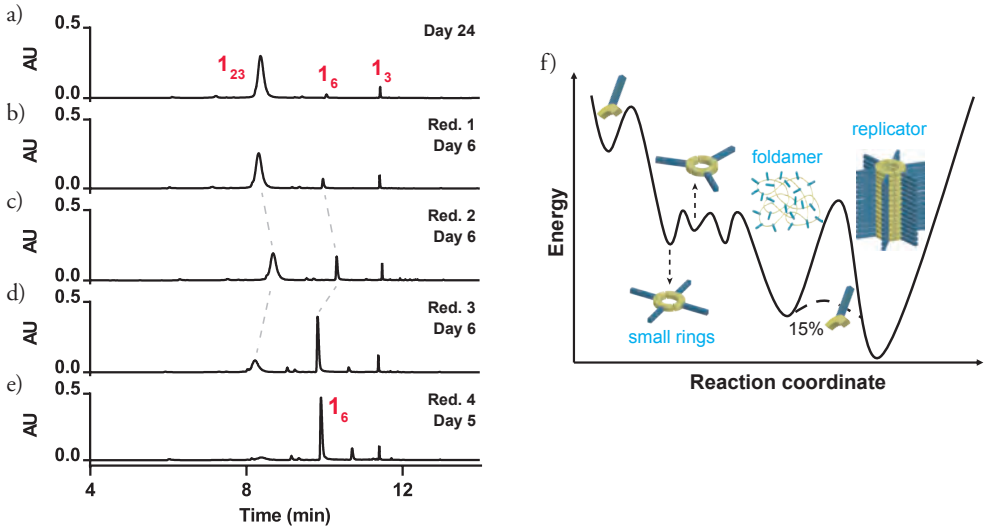

Figure 4.6 UPLC analyses of a DCL made from **1** (2.0 mM) in borate buffer (12.5 mM, pH = 8.0): **a)** after stirring for 24 days; after stirring for 6 days following **b)** the first reduction, **c)** the second reduction; **d)** the third reduction, and **e)** after stirring for 5 days following the fourth reduction. DTT was used as a reducing agent, and the library was reduced in each step, approximately 5-15%. **f)** Schematic representation of the energy diagram of the dynamic transition from small to folded and self-replicating structures based on building block **1**, upon complete oxidation and subsequent series of partial reduction/oxidation steps.

4.3 Conclusions

In conclusion, the above-discussed results suggest that dynamic combinatorial chemistry is a powerful approach to access both synthetic foldamers and self-replicators, from single monomers with limited information content. However, the exact prediction of the outcome of a DCL based on the chemical structure of a building block remains a challenge. We observe that the design criteria for molecules which oligomerize to yield foldamers are remarkably similar to those that result in self-replicator formation. In fact, a relatively small change at the C-terminus of the peptide chain (a hydrazide group

instead of a carboxyl group) directed the system from preferentially being governed by *intra*molecular (within the same oligomer to cause folding) to *inter*molecular non-covalent interactions (between different but identical oligomers to cause self-assembly driven self-replication).

The monomers' resemblance that spontaneously organize into discrete folded structures and self-replicators suggests that these processes are related. Thus, the possibility of these systems to undergo a conversion of one type of assembly into another was investigated by employing different strategies. Foldamers from building blocks that preferentially result in self-replicator formation (**4**) were obtained only in combination with molecule **1**, which independently can self-assemble into a large macrocycle with defined folded conformation. Other approaches that focus on modifying the experimental conditions of DCLs made only of **4** did not result in foldamer formation. In contrast, the *in situ* reconfigurations from foldamer towards self-replicator is possible, as shown by the stepwise, partial reductions of DCL dominated by $\mathbf{1}_{23}$. The ability of an initially foldamer-dominated system to undergo dynamic transformation ($\mathbf{1}_{23} \rightarrow \mathbf{1}_{6}$), while the opposite is not feasible ($\mathbf{4}_{6} \rightarrow$ **foldamer**), indicates that foldamers are transiently durable and trapped in a local minimum, while self-replicators are likely to persist for a long time due to their thermodynamic stability. Upon inputting the activation energy, in this case, incremental reductions, the foldamer was converted to a more stable structure, i.e., the self-replicator.

The relationship between the folding and formation of fibrillar assemblies, as observed in this work, shares resemblance with some systems present in nature. For example, amyloid beta (Aβ) peptide, when misfolded, aggregates to form plaques of fibrils found in the brains of people with Alzheimer's disease.[24] Here, when given the opportunity (partially reduced and in the presence of a small amount of $\mathbf{1}_{6}$ seed), the system undergoes the transition from the protein-like structure into the thermodynamically most stable state, fibrillar self-replicator.

4.4 Acknowledgments

Dr. C. G. Pappas is recognized for the conception of the project and gratefully acknowledged for the discussion of results. A. Kiani and J. Ottelé are acknowledged for negative staining TEM imaging. Dr. C. G. Pappas is recognized for proof-reading this chapter and giving valuable feedback.

4.5 Materials and Methods

4.5.1 Materials

Building blocks **4**, **5** and **6** were purchased from GenScript Biotech (Piscataway, New Jersey, USA) and prepared by coupling 3,5-bis(tritylthio)benzoic acid, which was synthesized via a previously reported procedure[22] at the N-terminus. Boric anhydride (Sigma-Aldrich) and sodium hydroxide (Merck Chemicals) were utilized for buffer preparation and pH adjustments. The concentration of borate buffer is given in $B_4O_7^{2-}$ ions. Thioflavin T was purchased from Sigma-Aldrich and used for fluorescence assays. Acetonitrile (UPLC-MS grade), water (UPLC-MS grade), and trifluoroacetic acid (HPLC grade) were purchased from Biosolve BV and used for UPLC measurements. Doubly distilled water was used in all experiments.

4.5.2 Library Preparation and Sampling

Building blocks were dissolved to a concentration of 4.0 mM in borate buffer (50 mM in $B_4O_7^{2-}$, pH 8.2). As peptide molecules are salts of TFA, the pH value had to be readjusted to 8.2 with 1 M NaOH. Subsequently, the solution was oxidized to 65-80% with sodium perborate solution (40 mM). The sample was equilibrated in a UPLC vial (12 x 32 mm) with a Teflon-coated screw cap. The UPLC vial was equipped with a cylindrical stirring bar (2 x 5 mm, purchased from VWR), and the solution was stirred at 1200 rpm using an IKA C-MAG HS 7 control hot plate stirrer. The temperature was kept constant at 25°C using a Thermo Scientific Compact Digital Dry Bath. The composition of libraries was monitored by sampling 5 μL of the DCL and diluting it to 50 μL with doubly distilled water, followed by analysis using UPLC.

4.5.3 Seeding Experiments

Peptides **4**-**6** (4.0 mM, 50.0 mM borate buffer, pH 8.2) were oxidized with freshly prepared sodium perborate solution (40 mM) so that the sample contained mostly monomer and non-assembled macrocycles (trimer, tetramer, etc.), and then split into two. To one half of the libraries of each peptide building block, a small amount (15 mol%) of a previously prepared solution containing predominantly self-assemblies of the corresponding macrocycle was added. All libraries were stirred at 1200 rpm, kept at a constant temperature of 25°C and monitored with UPLC and UPLC/MS.

4.5.4 Circular Dichroism (CD)

Samples were prepared by diluting libraries to 0.4 mM (with respect to monomer building block concentration). All spectra were recorded on a JASCO J-715 CD spectrophotometer using HELMA quartz cuvettes with a path length of 1.0 mm. Continuous spectra were obtained from 200 nm to 400 nm at room temperature. All reported spectra were an average of three scans recorded at a scan rate of 200 nm/min with a 2-nm step interval and measured in millidegrees. Solvent spectra were subtracted from all spectra.

4.5.5 Thioflavin T (ThT) Fluorescence Assay

A ThT stock solution (2.2 mM) was prepared in 10 mL borate buffer (50.0 mM, pH 8.2) and filtered through a 0.2 μm syringe filter. A working solution (22 μM) was freshly prepared on the day of analysis by diluting 50 μL of the stock solution into 5 mL borate buffer (50.0 mM, pH 8.2). The fluorescence intensity of 450 μL ThT solution was measured by excitation at 440 nm (slit width 10 nm) and emission between 460-700 nm (slit width 10 nm), averaging 3 accumulations. An aliquot of 100 μL of peptide solution in borate buffer was added to the HELMA 10x2 mm quartz cuvette, incubated for 2 min, and the intensity was measured over 3 accumulations. All fluorescence measurements were recorded on a JASCO FP6200 fluorimeter at room temperature.

4.5.6 Atomic Force Microscopy (AFM)

AFM samples were prepared by depositing 100 μL of a sample (diluted to 10 μM concentration in peptide building blocks **4**-**6** with UPLC water) onto a clean mica surface (Grade V1, Van Loenen Instruments). Subsequently, the excess solvent was removed by blotting into a piece of paper, and the surface was washed twice with 100 μL UPLC grade water, blotted into a piece of paper and finally dried in a gentle stream of air. The AFM measurements have been performed using a Bruker Multimode 8 instrument in ScanAsyst-Air imaging mode. Measurements were performed in air at room temperature. As a probe, a ScanAsyst Air (Bruker) silicon tip on a nitride cantilever was used with the following parameters: length: 115 μm, width: 25 μm, resonance frequency: 70 kHz, force constant: 0.4 N/m. The images were recorded with frequencies between 0.5 and 1.5 Hz and analyzed with NanoScope Analysis 1.50 software (Bruker Corporation, 2015).

4.5.7 Negative Staining Transmission Electron Microscopy (TEM)

A 5 μL drop of the sample was deposited on a 400-mesh copper grid covered with a thin carbon film (Agar Scientific). After 30 s, the droplet was blotted on filter paper. The sample was then stained twice (4 μL each time) with a solution of 2% uranyl acetate deposited on the grid and blotted on the filter paper immediately after the first deposition and 30 s after the second deposition. The grids were observed in a Philips CM12 electron microscope operating at 120 kV. Images were recorded on a slow-scan CCD camera.

4.6 UPLC and UPLC/MS Analyses

UPLC measurements were performed on a Waters Acquity UPLC H-class or H+-class system equipped with a PDA detector. UPLC analyses were performed on an Acquity UPLC Peptide CSH C18 column, purchased from Waters, or an Aeris XB-C18 column, purchased from Phenomenex, both 1.7 mm (150 x 2.1 mm), using UPLC-MS grade water (eluent **A**) and UPLC-MS grade acetonitrile (eluent **B**), containing 0.1 V/V % TFA as a modifier. A flow rate of 0.3 mL/min and a column temperature of 35°C were applied. Spectra were recorded at a detection wavelength of 254 nm. UPLC-MS measurements were performed using a Waters Acquity UPLC H-class system coupled to Waters Xevo-G2 TOF. The mass spectrometer was operated in positive electrospray ionization mode with the following ionization parameters: capillary voltage: 3 kV, sampling cone voltage: 20 V, extraction cone voltage: 4 V, source gas temperature: 120°C, desolvation gas temperature: 450°C, cone gas flow (nitrogen): 1 L/h, desolvation gas flow (nitrogen): 800 L/h.

4.6.1 UPLC Methods

Method 1		
t (min)	A (%)	B (%)
0.00	90.0	10.0
1.00	85.0	15.0
11.00	50.0	50.0
13.00	5.0	95.0
13.50	5.0	95.0
14.00	90.0	10.0
17.00	90.0	10.0

Method 2		
t (min)	A (%)	B (%)
0.00	90.0	10.0
1.00	85.0	15.0
9.00	76.0	24.0
12.50	40.0	60.0
13.00	5.0	95.0
13.50	5.0	95.0
14.00	90.0	10.0
17.00	90.0	10.0

Table S4.1 UPLC method 1 for the analysis of DCLs reported from **Section 4.2.2** to **Section 4.2.4.2** and UPLC method 2 for the analysis of DCL reported in **Sections 4.2.4.3** and **4.2.5**.

4.6.2.1 UPLC and UPLC/MS Analysis of DCL Made From 4

Species	Elution Time (min)	
	UPLC	*UPLC/MS*
4	3.87	4.36
$\mathbf{4}_4$	3.92	4.53
$\mathbf{x}_1$	4.23	4.91
$\mathbf{4}_6$	4.38	5.04
$\mathbf{x}_2$	4.58	5.21
linear $\mathbf{4}_2$	4.75	5.35
$\mathbf{4}_3$	5.07	5.67

Table S4.2 Elution times (in the UPLC and UPLC/MS chromatograms) of species formed through oxidation and exchange of a DCL made from **4**.

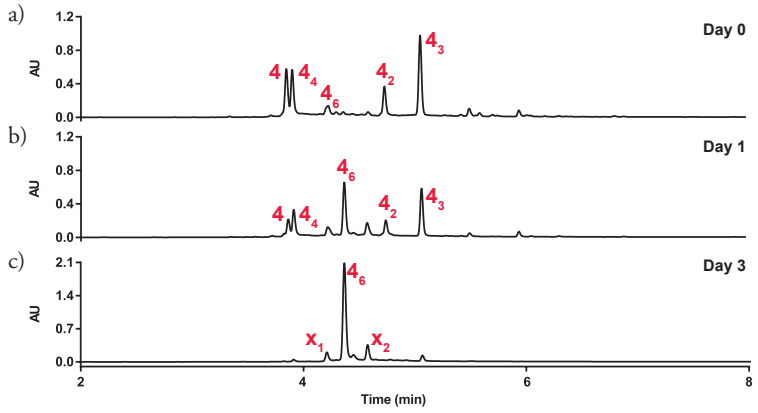

Figure S4.1 Relevant parts of the UPLC traces (monitored at 254 nm) recorded at **a)** day 0, **b)** day 1 and **c)** day 3 of the product mixture obtained by oxidation of peptide **4** (4.0 mM) in borate buffer (50.0 mM, pH 8.2); $NaBO_3$ mediated oxidation of 80% monomer at day 0, subsequent oxidation by air. $\mathbf{x}_1$ and $\mathbf{x}_2$ correspond to unidentified products, which could not be assigned to any of the macrocycles that can be produced by peptide **4** and are probably macrocycles of deletion product(s) or other impurities containing the 3,5-mercaptobenzoic acid unit.

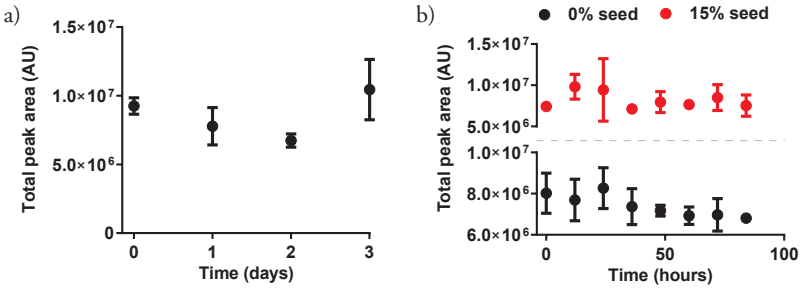

Figure S4.2 a) Total peak area of DCLs made from building block **4** (4.0 mM) in borate buffer (50.0 mM, pH 8.2), stirred at 1200 rpm. Libraries were oxidized to approximately 80% with respect to monomer. **b)** The total peak area of non-seeded (**bottom**) and seeded libraries (15 mol% of seed, **top**) made from molecule **4**. Libraries were prepared at 4.0 mM concentration in building block **4**, in borate buffer (50.0 mM, pH 8.2), and stirred at 1200 rpm. The seed was added to the library oxidized to approximately 75% with respect to monomer. The temperature was kept constant at 25°C throughout all experiments. The graphs are based on 3 independent replicates.

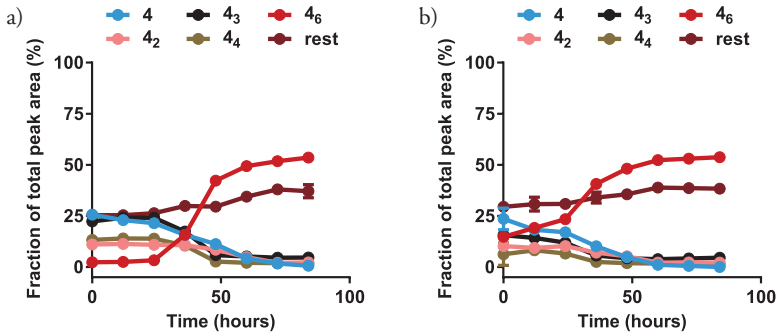

Figure S4.3 Kinetic profile of formation of $\mathbf{4}_6$ in **a)** a non-seeded and **b)** a seeded library with 15 mol%, starting from building block **4** (4.0 mM) in borate buffer (50.0 mM, pH 8.2), stirred at 1200 rpm. The seed was added to the library oxidized to approximately 75% with respect to monomer. The temperature was kept constant at 25°C throughout all experiments.

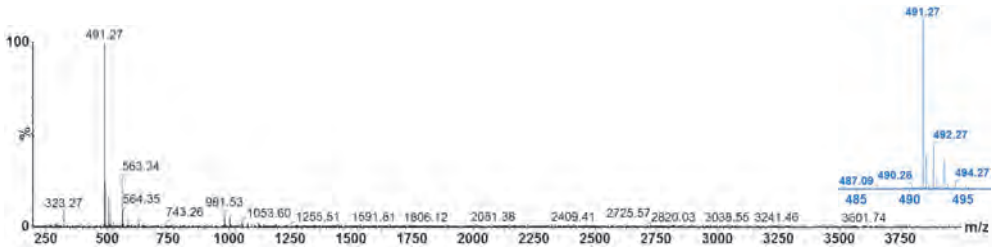

Figure S4.4 Mass spectrum of **4** (t_R = 4.36 min) from the LC-MS analysis of a DCL made from **4**. m/z calculated: 491.18 $[M+H]^+$; m/z observed: 491.27 $[M+H]^+$.

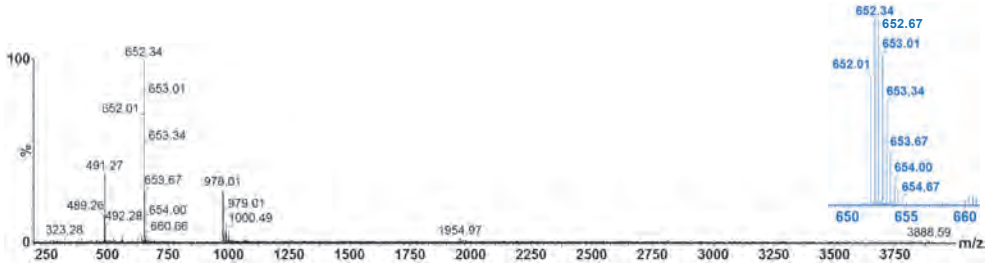

Figure S4.5 Mass spectrum of $\mathbf{4}_4$ (t_R = 4.53 min) from the LC-MS analysis of a DCL made from **4**. m/z calculated: 977.36 $[M+2H]^{2+}$, 651.91 $[M+3H]^{3+}$; m/z observed: 977.51 $[M+2H]^{2+}$, 652.01 $[M+3H]^{3+}$;

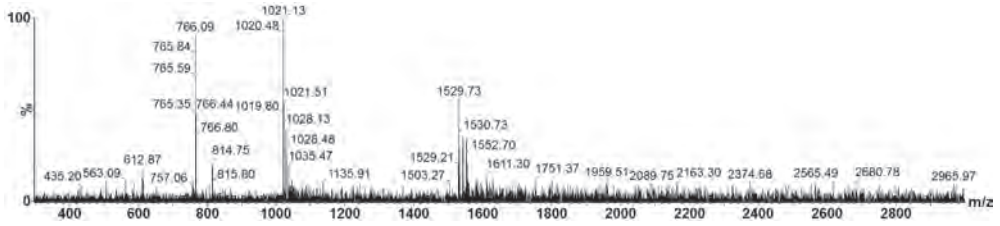

Figure S4.6 Mass spectrum of $\mathbf{x}_1$ (t_R = 4.91 min) from the LC-MS analysis of a DCL made from **4**. m/z observed: 1529.73 $[M+2H]^{2+}$, 1019.80 $[M+3H]^{3+}$, 765.35 $[M+4H]^{4+}$.

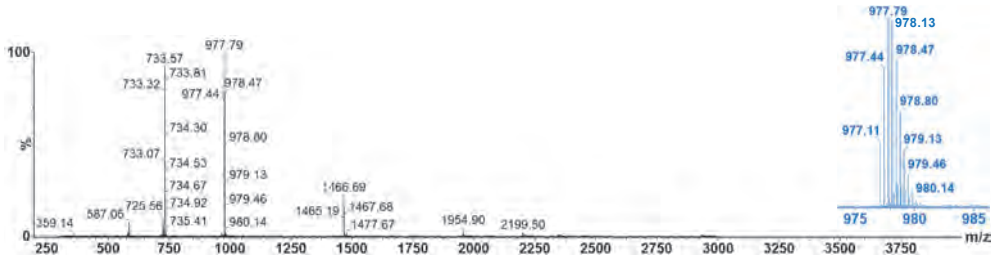

Figure S4.7 Mass spectrum of $\mathbf{4}_6$ (t_R = 5.04 min) from the LC-MS analysis of a DCL made from **4**. m/z calculated: 1465.54 $[M+2H]^{2+}$, 977.36 $[M+3H]^{3+}$, 733.27 $[M+4H]^{4+}$; m/z observed: 1465.19 $[M+2H]^{2+}$, 977.11 $[M+3H]^{3+}$, 733.07 $[M+4H]^{4+}$.

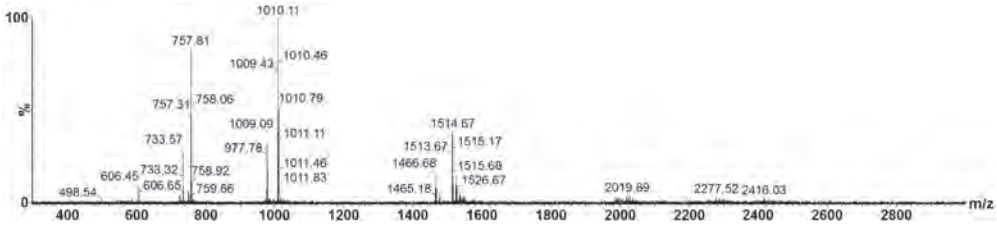

Figure S4.8 Mass spectrum of $\mathbf{x}_2$ (t_R = 5.21 min) from the LC-MS analysis of a DCL made from **4**. m/z observed: 1513.16 $[M+2H]^{2+}$, 1009.09 $[M+3H]^{3+}$, 757.31 $[M+4H]^{4+}$.

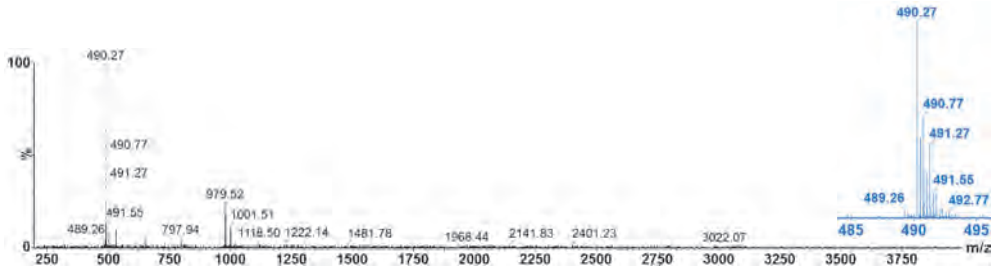

Figure S4.9 Mass spectrum of **linear** $\mathbf{4}_2$ (t_R = 5.35 min) from the LC-MS analysis of a DCL made from **4**. m/z calculated: 490.18 $[M+2H]^{2+}$; m/z observed: 490.27 $[M+2H]^{2+}$.

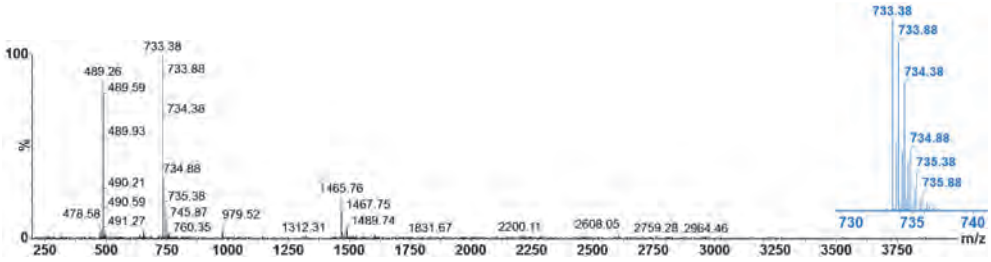

Figure S4.10 Mass spectrum of $\mathbf{4}_3$ (t_R = 5.67 min) from the LC-MS analysis of a DCL made from **4**. m/z calculated: 1465.54 $[M+H]^+$, 733.27 $[M+2H]^{2+}$, 489.18 $[M+3H]^{3+}$; m/z observed: 1465.76 $[M+H]^+$, 733.38 $[M+2H]^{2+}$, 489.26 $[M+3H]^{3+}$.

4.6.2.2 UPLC and UPLC/MS Analysis of DCL Made From 5

Species	Elution Time (min)	
	UPLC	*UPLC/MS*
sulfoxide of 5	3.75	4.03
5	6.00	6.32
5_4	6.10	6.43
5_5	6.19	6.51
linear 5_2	6.98	7.29
5_3	7.23	7.54

Table S4.3 Elution times (in the UPLC and UPLC/MS chromatograms) of species formed through oxidation and exchange of a DCL made from **5**.

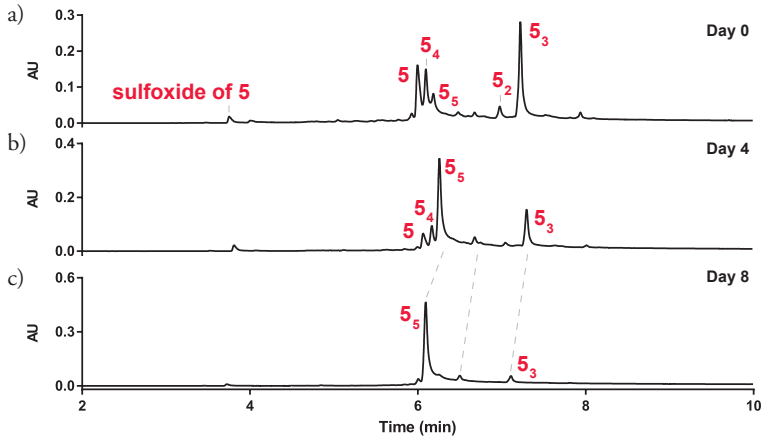

Figure S4.11 Relevant parts of the UPLC traces (monitored at 254 nm) recorded at **a)** day 0, **b)** day 4 and **c)** day 8 of the product mixture obtained by oxidation of peptide **5** (4.0 mM) in borate buffer (50.0 mM, pH 8.2); $NaBO_3$ mediated oxidation of 80% monomer at day 0, subsequent oxidation by air.

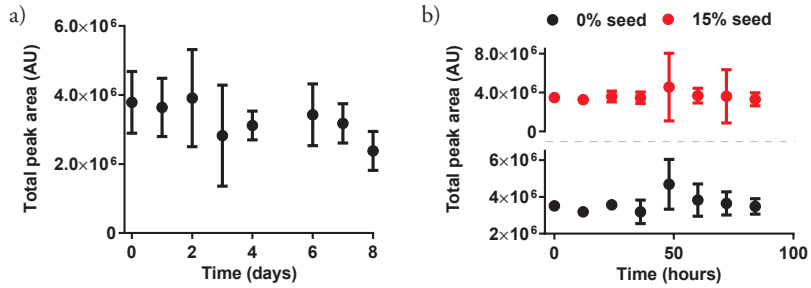

Figure S4.12 a) Total peak area of DCLs made from building block **5** (4.0 mM) in borate buffer (50.0 mM, pH 8.2), stirred at 1200 rpm. Libraries were oxidized to 80% with respect to monomer. **b)** The total peak area of non-seeded (**bottom**) and seeded libraries (15 mol% of seed, **top**) made from molecule **5**. Libraries were prepared at 4.0 mM concentration in building block **5**, in borate buffer (50.0 mM, pH 8.2) and stirred at 1200 rpm. The seed was added to the library oxidized to approximately 85% with respect to monomer. The temperature was kept constant at 25°C throughout all experiments. The graphs are based on 3 independent replicates.

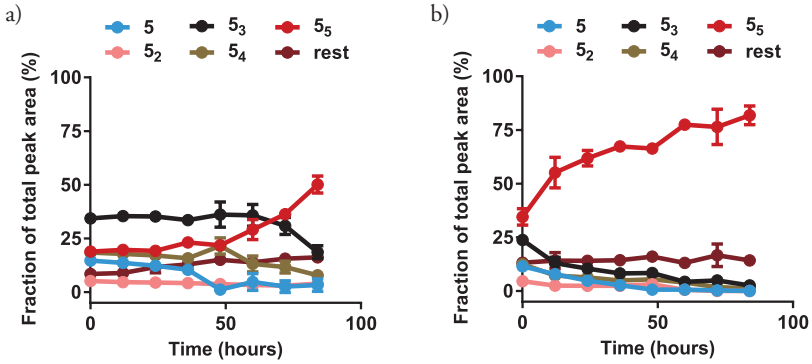

Figure S4.13 Kinetic profile of formation of $\mathbf{5}_5$ in **a)** a non-seeded and **b)** a seeded library with 15 mol%, starting from building block **5** (4.0 mM) in borate buffer (50.0 mM, pH 8.2), stirred at 1200 rpm. The seed was added to the library oxidized to approximately 85% with respect to monomer. The temperature was kept constant at 25°C throughout all experiments.

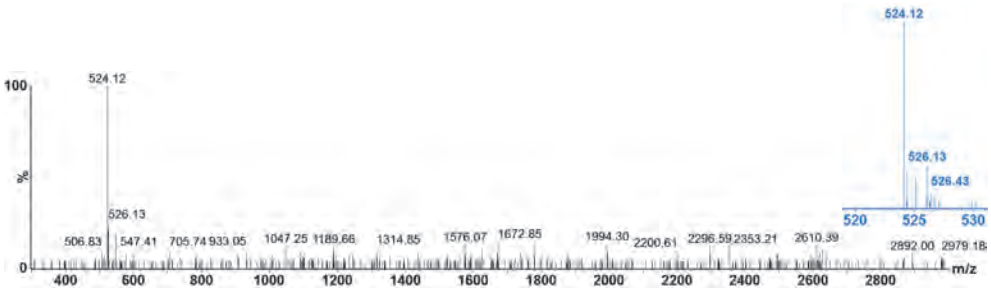

Figure S4.14 Mass spectrum of **sulfoxide of 5** (t_R = 4.03 min) from the LC-MS analysis of a DCL made from **5**. m/z calculated: 524.17 $[M+H]^+$; m/z observed: 524.12 $[M+H]^+$.

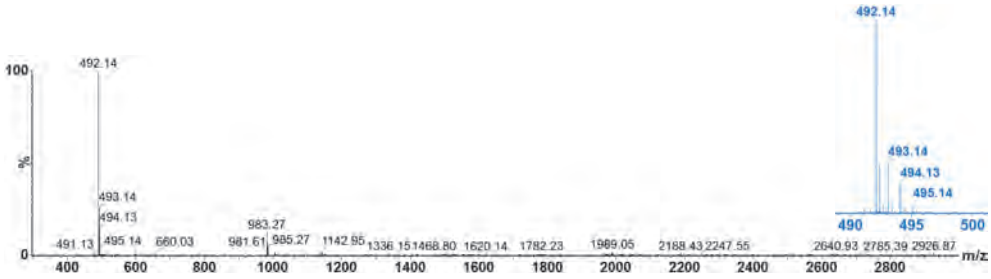

Figure S4.15 Mass spectrum of **5** (t_R = 6.32 min) from the LC-MS analysis of a DCL made from **5**. m/z calculated: 492.17 $[M+H]^+$; m/z observed: 492.14 $[M+H]^+$.

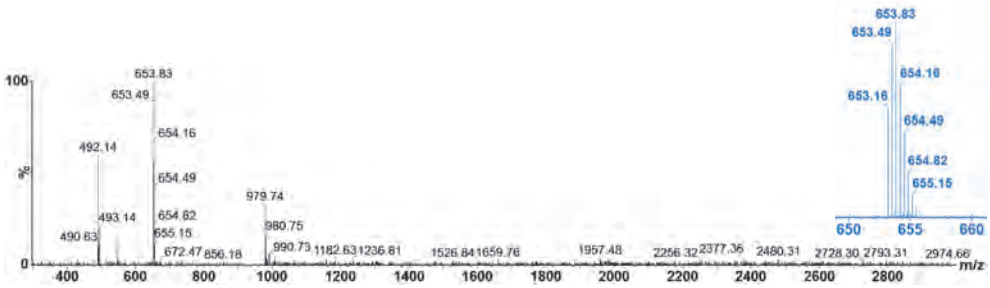

Figure S4.16 Mass spectrum of $\mathbf{5}_4$ (t_R = 6.43 min) from the LC-MS analysis of a DCL made from **5**. m/z calculated: 979.34 $[M+2H]^{2+}$, 653.23 $[M+3H]^{3+}$; m/z observed: 979.24 $[M+2H]^{2+}$, 653.16 $[M+3H]^{3+}$.

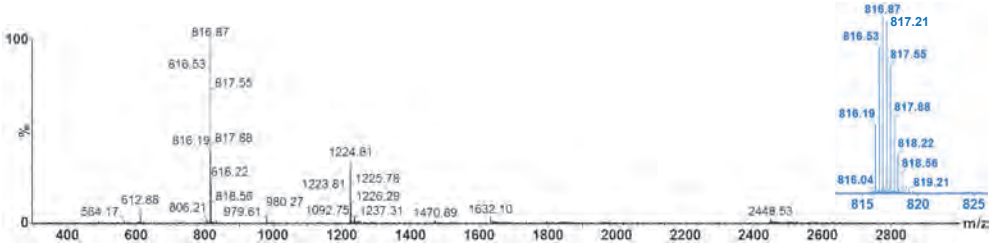

Figure S4.17 Mass spectrum of $\mathbf{5}_5$ (t_R = 6.51 min) from the LC-MS analysis of a DCL made from **5**. m/z calculated: 1223.93 $[M+2H]^{2+}$, 816.28 $[M+3H]^{3+}$, 612.46 $[M+4H]^{4+}$; m/z observed: 1223.81 $[M+2H]^{2+}$, 816.89 $[M+3H]^{3+}$, 612.64 $[M+4H]^{4+}$.

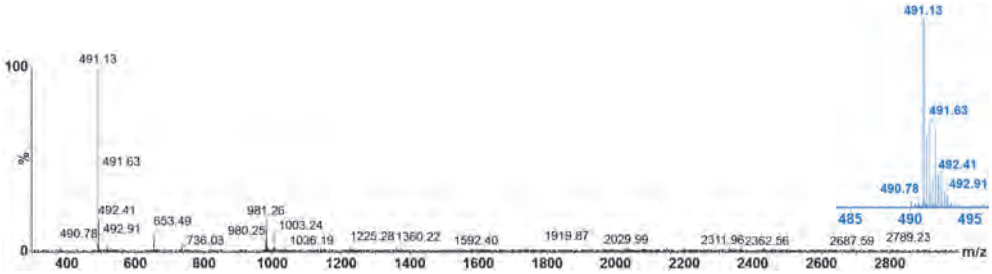

Figure S4.18 Mass spectrum of **linear** $\mathbf{5}_2$ (t_R = 7.29 min) from the LC-MS analysis of a DCL made from **5**. m/z calculated: 491.17 $[M+2H]^{2+}$; m/z observed: 491.13 $[M+2H]^{2+}$.

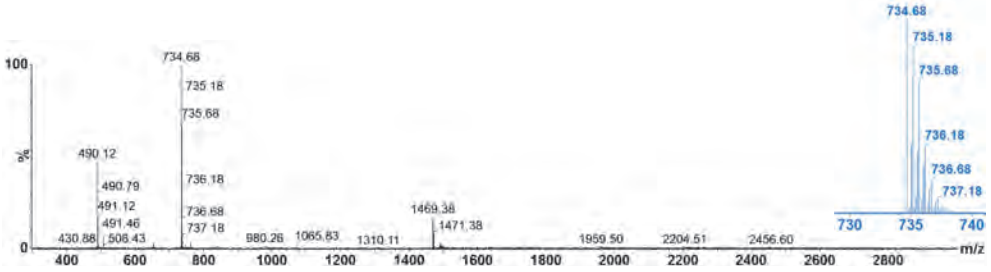

Figure S4.19 Mass spectrum of $\mathbf{5}_3$ (t_R = 7.54 min) from the LC-MS analysis of a DCL made from **5**. m/z calculated: 734.75 $[M+2H]^{2+}$, 490.17 $[M+3H]^{3+}$; m/z observed: 734.68 $[M+2H]^{2+}$, 490.12 $[M+3H]^{3+}$.

4.6.2.3 UPLC and UPLC/MS Analysis of DCL Made From 6

Species	Elution Time (min)	
	UPLC	*UPLC/MS*
sulfoxide of 6	3.01	3.21
6	5.55	5.77
6_4	5.75	6.03
6_5	6.17	6.40
6_6	6.33	6.57
linear 6_2	6.59	6.81
6_3	6.96	7.21

Table S4.4 Elution times (in the UPLC and UPLC/MS chromatograms) of species formed through oxidation and exchange of a DCL made from **6**.

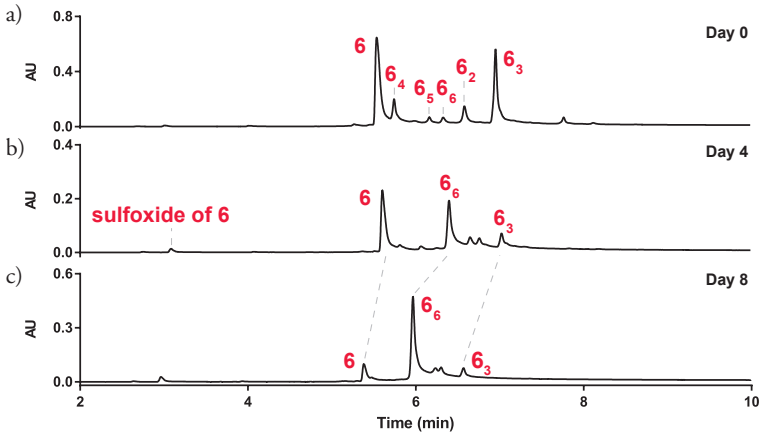

Figure S4.20 Relevant parts of the UPLC traces (monitored at 254 nm) recorded at **a)** day 0, **b)** day 4 and **c)** day 13; of the product mixture obtained by oxidation of peptide **6** (4.0 mM) in borate buffer (50.0 mM, pH 8.2); $NaBO_3$ mediated oxidation of approximately 60% monomer at day 0, subsequent oxidation by air.

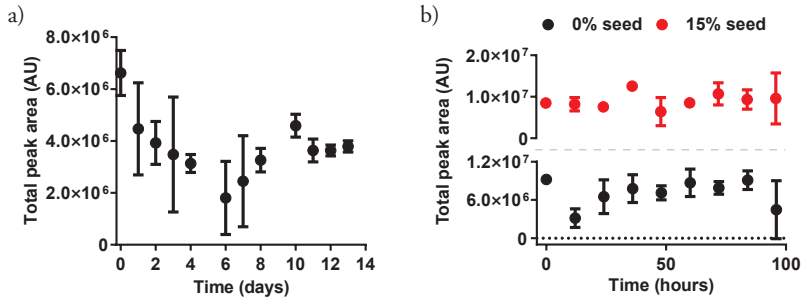

Figure S4.21 a) Total peak area of DCLs made from building block **6** (4.0 mM) in borate buffer (50.0 mM, pH 8.2), stirred at 1200 rpm. Libraries were oxidized to approximately 60% with respect to monomer. **b)** The total peak area of $\mathbf{6}_6$ specie in non-seeded (**bottom**) and seeded libraries (15 mol% of seed, **top**) made from molecule **6**. Libraries were prepared at 4.0 mM concentration in building block **6**, in borate buffer (50.0 mM, pH 8.2), and stirred at 1200 rpm. The seed was added to the library oxidized to approximately 75% with respect to monomer. The temperature was kept constant at 25°C throughout all experiments. The graphs are based on 3 independent replicates.

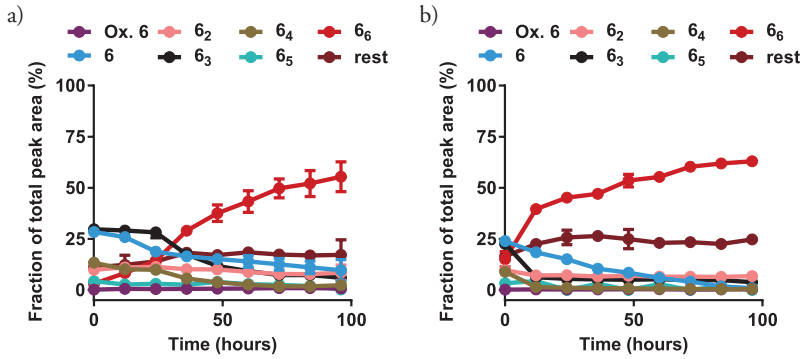

Figure S4.22 Kinetic profile of formation of $\mathbf{6}_6$ in **a)** a non-seeded and **b)** a seeded library with 15 mol%, starting from building block **6** (4.0 mM) in borate buffer (50.0 mM pH 8.2), stirred at 1200 rpm. The seed was added to the library oxidized to approximately 75% with respect to monomer. The temperature was kept constant at 25°C throughout all experiments.

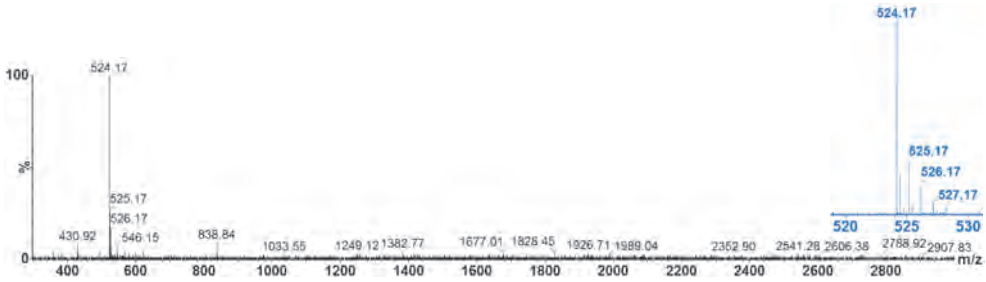

Figure S4.23 Mass spectrum of **sulfoxide of 6** (t_R = 3.21 min) from the LC-MS analysis of a DCL made from **6**. m/z calculated: 524.17 $[M+H]^+$; m/z observed: 524.17 $[M+H]^+$.

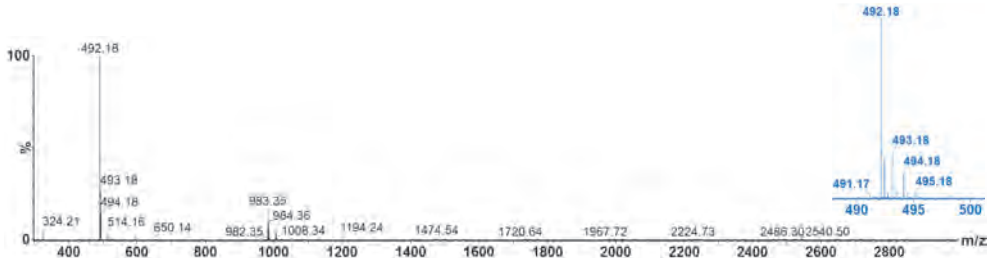

Figure S4.24 Mass spectrum of **6** (t_R = 5.77 min) from the LC-MS analysis of a DCL made from **6**. m/z calculated: 492.17 $[M+H]^+$; m/z observed: 492.18 $[M+H]^+$.

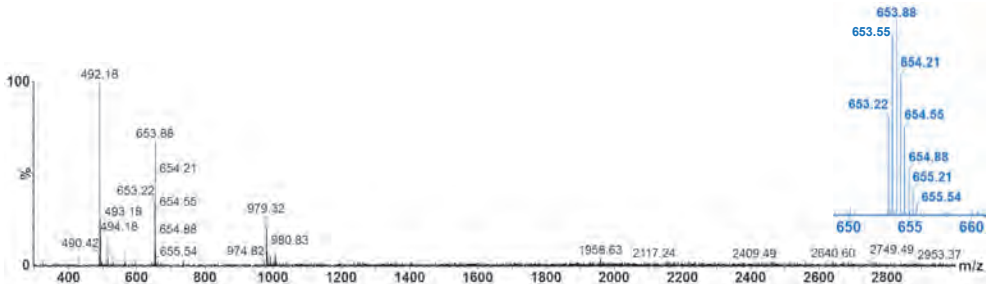

Figure S4.25 Mass spectrum of $\mathbf{6}_4$ (t_R = 6.03 min) from the LC-MS analysis of a DCL made from **6** m/z calculated: 979.34 $[M+2H]^{2+}$, 653.23 $[M+3H]^{3+}$; m/z observed: 979.32 $[M+2H]^{2+}$, 653.22 $[M+3H]^{3+}$.

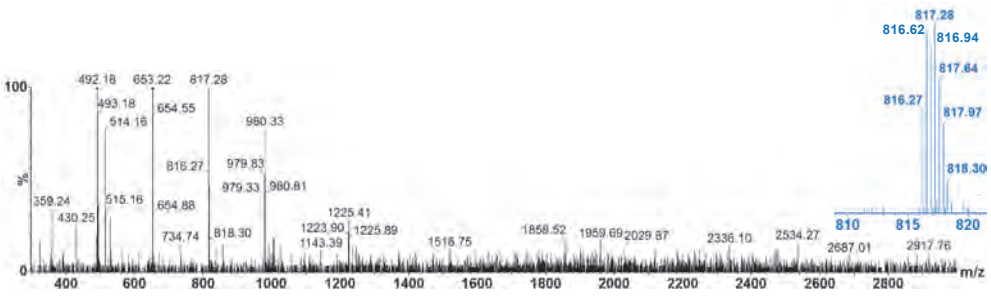

Figure S4.26 Mass spectrum of $\mathbf{6}_5$ (t_R = 6.40 min) from the LC-MS analysis of a DCL made from **6**. m/z calculated: 1223.93 $[M+2H]^{2+}$, 816.28 $[M+3H]^{3+}$; m/z observed: 1223.90 $[M+2H]^{2+}$, 816.27 $[M+3H]^{3+}$.

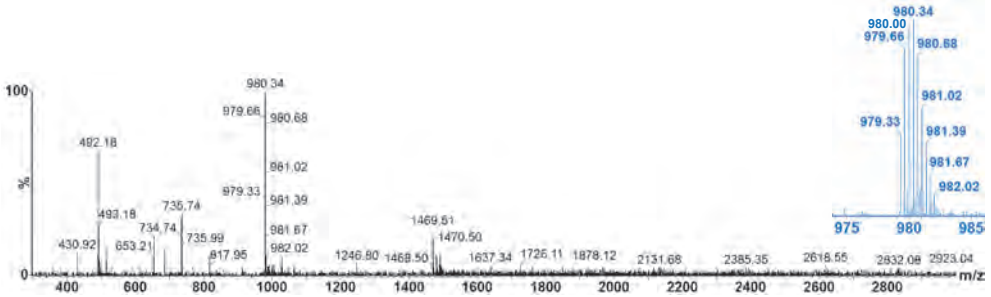

Figure S4.27 Mass spectrum of $\mathbf{6}_6$ (t_R = 6.57 min) from the LC-MS analysis of a DCL made from **6**. m/z calculated: 1468.51 $[M+2H]^{2+}$, 979.34 $[M+3H]^{3+}$, 734.76 $[M+4H]^{4+}$; m/z observed: 1468.50 $[M+2H]^{2+}$, 979.33 $[M+3H]^{3+}$, 734.74 $[M+4H]^{4+}$.

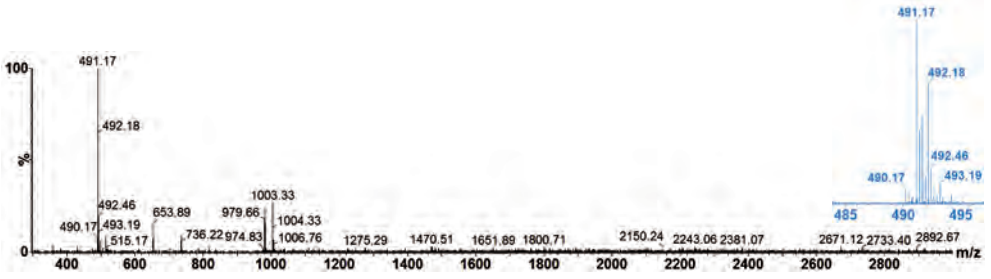

Figure S4.28 Mass spectrum of **linear** $\mathbf{6}_2$ (t_R = 6.81 min) from the LC-MS analysis of a DCL made from **6**. m/z calculated: 491.64 $[M+2H]^{2+}$; m/z observed: 491.17 $[M+2H]^{2+}$.

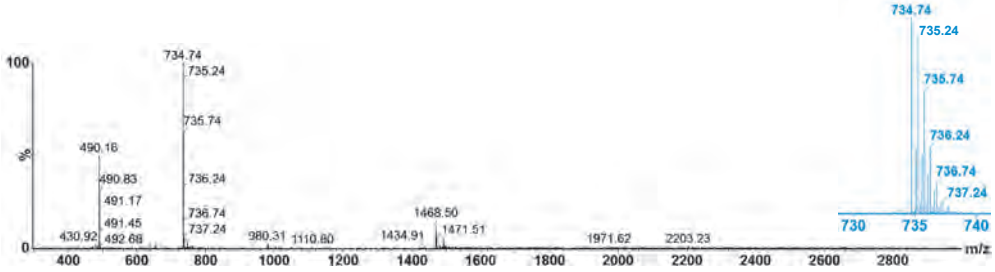

Figure S4.29 Mass spectrum of $\mathbf{6}_3$ (t_R = 7.21 min) from the LC-MS analysis of a DCL made from **6**. m/z calculated: 1467.51 $[M+H]^+$, 734.75 $[M+2H]^{2+}$, 490.17 $[M+3H]^{3+}$; m/z observed: 1468.50 $[M+H]^+$, 734.74 $[M+2H]^{2+}$, 490.16 $[M+3H]^{3+}$.

4.6.2.4 UPLC and UPLC/MS Analysis of DCLs Made From 4, 5 or 6 in Presence of Different Salts

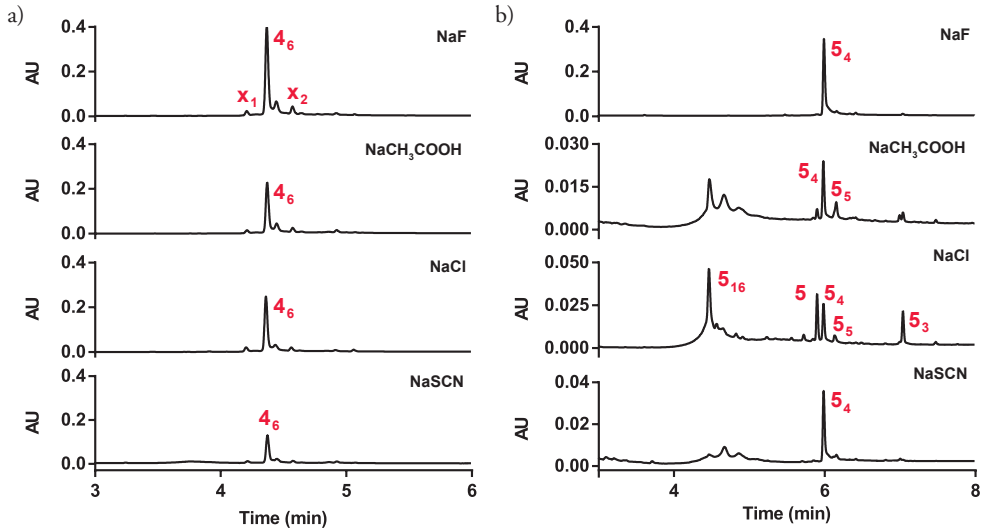

Figure S4.30 UPLC analyses of DCLs made from **a) 4** (4.0 mM) and **b) 5** (4.0 mM) in borate buffer (50.0 mM, pH 8.2) in the presence of 1 M NaF, $NaCH_3COO$, NaCl and Na SCN (from top to bottom) after stirring for 19 days.

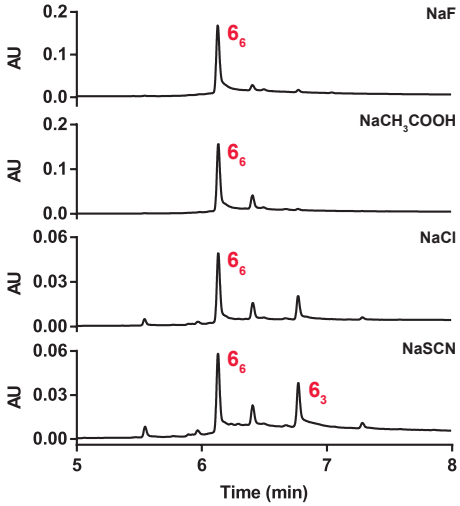

Figure S4.31 UPLC analyses of DCLs made from **6** (4.0 mM) in borate buffer (50.0 mM, pH 8.2) in the presence of 1 M NaF, $NaCH_3COO$, NaCl and Na SCN (from top to bottom) after stirring for 19 days.

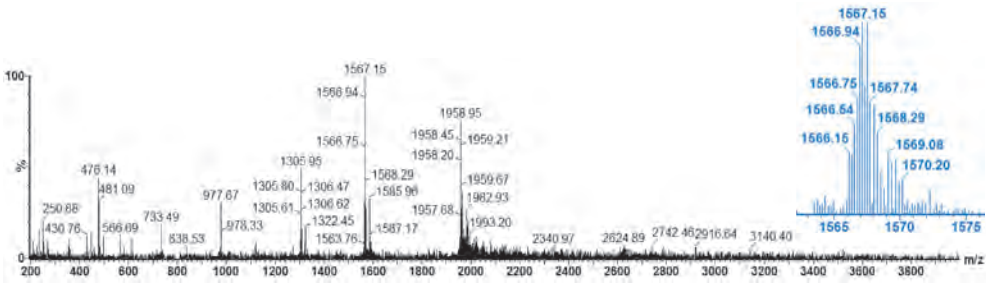

Figure S4.32 Mass spectrum of $\mathbf{5}_{16}$ (t_R = 5.38 min) from the LC-MS analysis of a DCL made from **5**. m/z calculated: 1957.68 $[M+4H]^{4+}$, 1566.34 $[M+5H]^{5+}$, 1305.45 $[M+6H]^{6+}$; m/z observed: 1957.45 $[M+4H]^{4+}$, 1566.15 $[M+5H]^{5+}$, 1305.29 $[M+6H]^{6+}$.

4.6.2.5 UPLC/MS Analysis of DCL Made From 1 and 4

Species	Elution Time (min)	
	UPLC	*UPLC/MS*
$\mathbf{1}_4$	7.83	8.67
$(\mathbf{1})_n(\mathbf{4})_{23-n}$	8.00 – 9.12	8.85 – 10.50
$\mathbf{1}_3$	11.48	11.73

Table S4.5 Elution times (in the UPLC and UPLC/MS chromatograms) of species formed through oxidation and exchange of a DCL made from **1** and **4**. Mass spectra of species highlighted in blue are previously reported;[16] therefore, their mass spectra are not shown again.

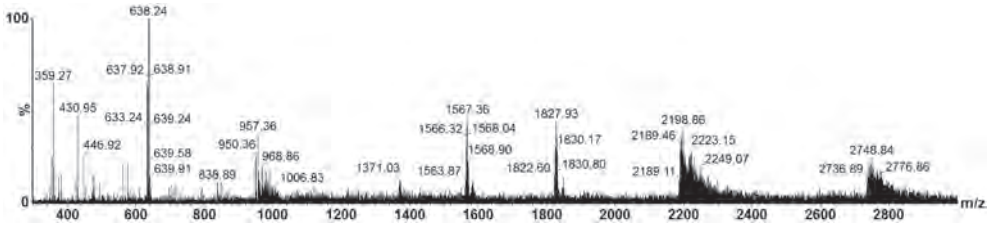

Figure S4.33 Mass spectrum of $\mathbf{1}_n\mathbf{4}_{23-n}$ (t_R = 8.85-10.50 min in **Figure 4.5**) from the LC-MS analysis of a DCL made from **1** and **4** (at a total concentration of 4.0 mM, 90:10 ratio). Due to the similarity of mass and close retention times of the different macrocycles, it is not possible to identify the exact composition. m/z calculated of mixed species $\mathbf{1}_n\mathbf{4}_{23-n}$ fall into the range of m/z observed. m/z calculated: 2731.43 – 2805.03 $[M+4H]^{4+}$, 2185.34 – 2244.22 $[M+5H]^{5+}$, 1821.28 – 1870.35 $[M+6H]^{6+}$, 1561.24 – 1603.30 $[M+7H]^{7+}$; m/z observed: 2732.39 – 2792.80 $[M+4H]^{4+}$, 2186.15 – 2244.14 $[M+5H]^{5+}$, 1822.01 – 1850.96 $[M+6H]^{6+}$, 1561.10 – 1592.65 $[M+7H]^{7+}$.

4.6.2.6 UPLC Analysis of DCL Made From 1 After Stepwise Reduction

Species	Elution Time (min)
	UPLC
1	5.89
$\mathbf{1}_4$	7.99
$\mathbf{1}_{23}$	8.18
$\mathbf{1}_6$	9.83
$\mathbf{1}_3$	11.37

Table S4.6 Elution times (in the UPLC and UPLC/MS chromatograms) of species formed through oxidation and exchange of a DCL made from **1**. Mass spectra of species highlighted in blue are previously reported;[16] therefore, their mass spectra are not shown again.

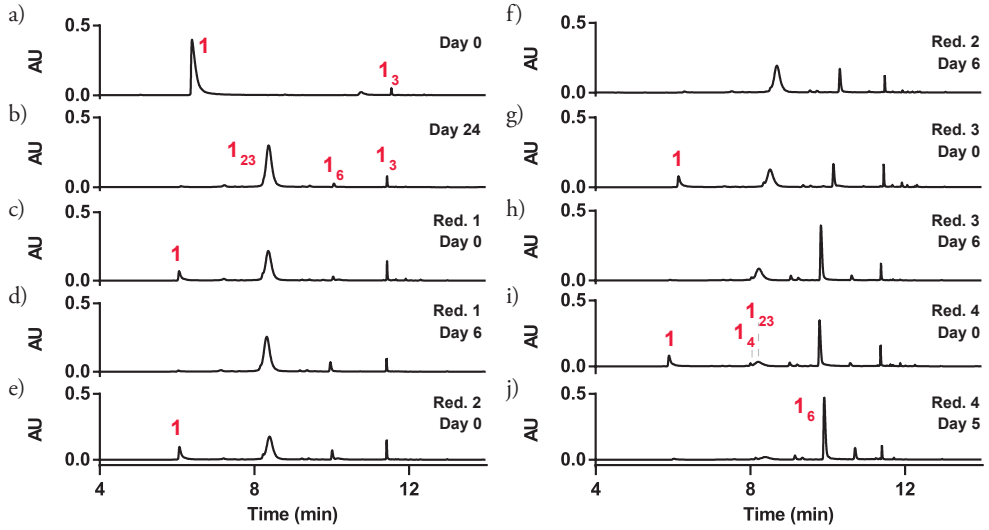

Figure S4.34 UPLC analyses of a DCL made from **1** (2.0 mM) in borate buffer (12.5 mM, pH = 8.0): **a)** right after dissolution of building block; **b)** after stirring for 24 days; after the first reduction on **c)** day 0 and **d)** day 6; after the second reduction on **e)** day 0 and **f)** day 6; after the third reduction on **g)** day 0 and **h)** day 6; after the fourth reduction on **i)** day 0 and **j)** day 5. DTT was used as a reducing agent, and the library was reduced in each step approximately 5-15%.

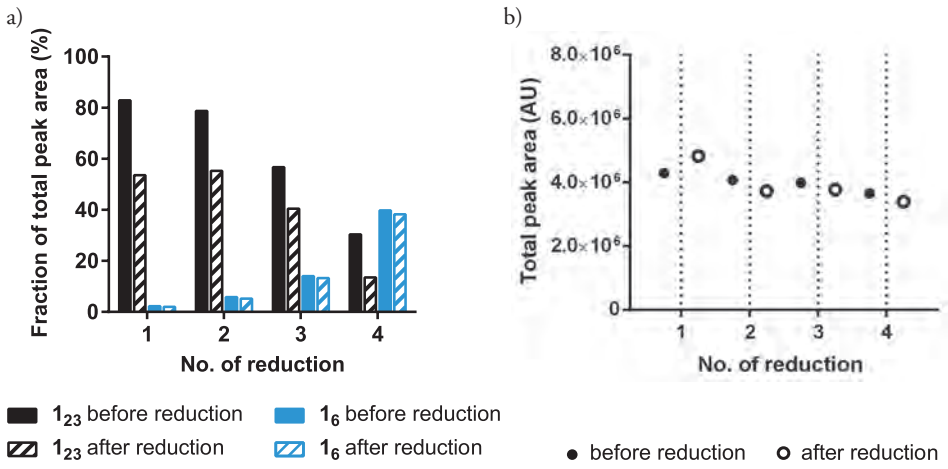

Figure S4.35 a) Fractions of total peak areas of $\mathbf{1}_{23}$ (black) and $\mathbf{1}_6$ (blue) before (fully colored bars) and after (stripped bars) each reduction step. **b)** Total peak area of DCLs made from building block **1** (4.0 mM) in borate buffer (12.5 mM, pH 8.0), stirred at 1200 rpm, before (full circles) and after (empty circles) each reduction step.

4.7 References

1 C. M. Runnels, K. A. Lanier, J. K. Williams, J. C. Bowman, A. S. Petrov, N. V. Hud, L. D. Williams, *J. Mol. Evol.* **2018**, *86*, 598-610.

2 N. Lahav, *Origins Life Evol. Biospheres,* **1993**, *23*, 329-344.

3 M. Frenkel-Pinter, M. Samanta, G. Ashkenasy, L. J. Leman, *Chem. Rev.* **2020**, *120*, 4707-4765.

4 F. Crick, *Nature*, **1970**, *227*, 561-563.

5 C. T. Walsh, *Posttranslational Modification of Proteins: Expanding Nature's Inventory*, Roberts and Company Publishers, Englewood, US, **2006.**

6 a) P. Adamski, M. Eleveld, A. Sood, A. Kun, A. Szilágyi, T. Czárán, E. Szathmáry, S. Otto, *Nat. Rev. Chem.* **2020**, *4*, 386-403; T. Kosikova, D. Philp, *Chem. Soc. Rev.* **2017**, *46*, 7274-7305; V. Patzke, G. von Kiedrowski, *Arkivoc*, **2007**, *5*, 293-310.

7 G. Guichard, I. Huc, *Chem. Commun.* **2011**, *47*, 5933-5941.

8 G. von Kiedrowski, *Angew. Chem. Ind. Ed.* **1986**, *25*, 932-935.

9 a) N. Paul, G. F. Joyce, *Proc. Natl. Acad. Sci. USA*, **2002**, *99*, 12733-12740; b) T. A. Lincoln, G. F. Joyce, *Science*, **2009**, 323, 1229-1232.

10 a) D. H. Lee, J. R. Granja, J. A. Martinez, K. Severin, M. R. Ghadiri, *Nature*, **1996**, *382*, 525-528; b) B. Rubinov, N. Wagner, M. Matmor, O. Regev, N. Ashkenasy, G. Ashkenasy, *ACS Nano*, **2012**, *6*, 7893-7901.

11 a) M. Malakoutikhah, J.-P. J. Peyralans, M. Colomb-Delsuc, H. Fanlo-Virgos, M. C. A. Stuart, S. Otto, *J. Am. Chem. Soc.* **2013**, *135*, 18406-18417; b) J. W. Sadownik, E. Mattia, P. Nowak, S. Otto, *Nat. Chem.* **2016**, *8*, 264-269.

12 C. M. Goodman, S. Choi, S. Shandler, W. F. DeGrado, *Nat. Chem. Biol.* **2007**, *3*, 252-262.

13 a) Z. C. Girvin, M. K. Andrews, X. Liu, S. H. Gellman, *Science* **2019**, *366*, 1528-1531; b) S. Kwon, A. Jeon, S. H. Yoo, I. S. Chung, H. S. Lee, *Angew. Chem. Int. Ed*. **2010**, *49*, 8232-8236.

14 a) P. E. Nielsen, M. Egholm, R. H. Berg, O. Buchardt, *Science*, **1991**, *254*, 1497-1500; b) D. H. Appella, L. A. Christianson, I. L. Karle, D. R. Powell, S. H. Gellman, *J. Am. Chem. Soc.* **1996**, *118*, 13071-13072; c) J. C. Nelson, J. G. Saven, J. S. Moore, P. G. Wolynes, Science, 1997, 277, 1793-1796; d) R. S. Lokey, B. L. Iverson, *Nature*, **1995**, *375*, 303-305; e) D. M. Bassani, J.-M. Lehn, G. Baum, D. Fenske, *Angew. Chem. Int. Ed.* **1997**, *36*, 1845-1847.

15 B. Liu, C. G. Pappas, E. Zangrando, N. Demitri, P. J. Chmielewski, S. Otto, *J. Am. Chem. Soc.* **2019**, 141, 1685-1689.

16 C. G. Pappas, P. K. Mandal, B. Liu, B. Kauffmann, X. Miao, D. Komáromy, W. Hoffmann, C. Manz, R. Chang, K. Liu, K. Pagel, I. Huc, S. Otto, *Nat. Chem.* **2020**, 12, 1180-1186.

17 C. G. Pappas, B. Liu, I. Marić, J. Ottelé, A. Kiani, M. L. van der Klok, P. R. Onck, S. Otto, Two Sides of the Same Coin: Emergence of Foldamers and Self-Replicators from Dynamic Combinatorial Libraries, Unpublished results.

18 B. Liu, Folding and Replication in Complex Dynamic Molecular Networks, Doctoral dissertation, University of Groningen, **2019**, pp 189-214.

19 A. Dirksen, S. Dirksen, T. M. Hackeng, P. E.

Dawson, *J. Am. Chem. Soc.* **2006**, *128*, 15602-15603.

20 a) S. Raddatz, J. Mueller-Ibeler, J. Kluge, L. Wäß, G. Burdinski, J. R. Havens, T. J. Onofrey, D. Wang, M. Schweitzer, *Nucleic Acids Res.* **2002**, *30*, 4793-4802; b) X. Zhang, *Molecules* **2020**, *25*, 1-15.

21 P. W. J. M. Frederix, J. Idé, Y. Altay, G. Schaeffer, M. Surin, D. Beljonne, A. S. Bondarenko, T. L. C. Jansen, S. Otto, S. J. Marrink, *ACS Nano.* **2017**, *11*, 7858-7868.

22 J. M. A. Carnall, C. A. Waudby, A. M. Belenguer, M. C. A. Stuart, J. J.-P. Peyralans, S. Otto, *Science* **2010**, *327*, 1502-1506.

23 a) W. Melander, C. Horváth, *Arch. Biochem. Biophys*, **1977**, *183*, 200-215; b) N. Ponnuswamy, F. B. L. Cougnon, J. M. Clough, G. D. Pantoş, J. K. M. Sanders, *Science* **2012**, 338, 783-785.

24 C. L. Masters, D. J. Selkoe, *Cold. Spring. Harb. Perspect. Med.* **2012**, *2*, 1-24.